Effects of Hydrogen in Working Gas on Valence States of Oxygen in Sputter-Deposited Indium Tin Oxide Thin Films

Suning Luo,[†,‡] Shigemi Kohiki,[*,†] Koichi Okada,[†] Atsushi Kohno,[§] Takayuki Tajiri,[§] Masao Arai,[||] Satoshi Ishii,[⊥] Daiichiro Sekiba,[⊥] Masanori Mitome,[||] and Fumiya Shoji[#]

Department of Materials Science, Kyushu Institute of Technology, 1-1 Sensui, Tobata, Kitakyushu 804-8550, Japan, Liaoning Institute of Technology, No.169 Shiying Street, Jinzhou 121001, Liaoning, China, Department of Applied Physics, Fukuoka University, 8-19-1 Nanakuma, Jonan, Fukuoka 814-0180, Japan, National Institute for Materials Science, 1-1 Namiki, Tsukuba, Ibaraki 305-0044, Japan, Tandem Accelerator Complex, University of Tsukuba, 1-1-1 Tennodai, Tsukuba, Ibaraki 305-8577, Japan, and Kyushu Kyoritsu University, 1-8 Jiyugaoka, Yahatanishi, Kitakyushu 807-8585, Japan

ABSTRACT X-ray photoelectron spectroscopy (XPS) and Rutherford backscattering spectroscopy—elastic recoil detection analysis (RBS—ERDA) revealed that hydrogen in working gas for dc-plasma sputter deposition resided in indium tin oxide (ITO) films and generated the O^- state seen as the suboxide-like O 1s peak in XPS. Growth of the suboxide-like O 1s peak was parallel with an increase of the resided hydrogen quantified by RBS—ERDA. The first-principles band structure calculation revealed that the electronic structure of In_2O_3 crystal was realized typically for the most conductive as-deposited film grown in the gas containing hydrogen of 1 %. The as-deposited film grown in the gas containing hydrogen of more than 1 % exhibited rather high density but low mobility of carriers and showed the electronic structure above 4 eV originated from the O^- state due to the resided hydrogen in addition to that of the most conducting one. Both well preserved In_2O_3 band structure and proper concentration of the O^{2-} vacancy are indispensable for achieving the highest conductivity; however, the O^- state lowers efficiency of the carrier doping using the O^{2-} vacancy in the lattice and increases density of the ionized scattering center for the carriers.

KEYWORDS: hydrogen incorporation • sputter deposition • ITO thin film • X-ray photoelectron spectroscopy • Rutherford backscattering spectroscopy—elastic recoil detection analysis

INTRODUCTION

Indium tin oxide (ITO) has been the most widely used transparent conducting oxide in the electronic device industry (1—3). Thin film deposition of ITO without any heat treatments has been of great interest for next-generation device applications (4—6); however, it was reported that no substrate heating in deposition results in deteriorated characteristics such as amorphousness in crystallinity and lowering in both optical transparency and electrical conductivity of the films (7, 8). The optical and electrical properties depend on local environments of chemical bonds in the films. In crystalline ITO, n-type carriers are supplied from both oxygen vacancies (9, 10) and Sn^{4+} ions substituted for In^{3+} sites in the lattice, while in amorphous ITO oxygen vacancy is anticipated as a primary source of the carriers, because tin is not efficiently activated (11).

Koida et al. (12) prepared hydrogen-doped In_2O_3 films on glass substrate by rf-magnetron sputtering without any intentional substrate heating. For incorporation of hydrogen to the film, they introduced H_2O vapor into a chamber during the deposition. They revealed that the carriers of the as-deposited films were originated from doubly charged impurities, while those of the films annealed at 200 °C for 2 h in vacuum were resulted from singly charged impurities. King et al. (13) concluded that muonium forms a shallow donor center in In_2O_3 with the activation energy of 47 ± 6 meV. They suggested that hydrogen behaves as a shallow donor in In_2O_3. Limpijumnong et al. (14) clarified that hydrogen located at the interstitial sites and that substituted for the oxygen sites in In_2O_3 are shallow donors. Their first-principles calculation revealed that the oxygen vacancy in both the 2+ charged and neutral states are stable in In_2O_3, although the oxygen vacancy in the 1+ charged state is never stable. Therefore, the carriers from doubly charged impurities of the as-deposited hydrogen-doped films by Koida et al. (12) are due to the oxygen vacancy in In_2O_3, and those from singly charged impurities of the films annealed in vacuum are due to hydrogen at the interstitial sites and/or hydrogen substituted for the oxygen sites in In_2O_3.

We reported that hydrogen with the concentration of 1 % in working gas resulted in the highest conductivity and the transparency larger than 80 % in visible wavelength region

* To whom correspondence should be addressed. E-mail: kohiki@che.kyutech.ac.jp.
Received for review October 3, 2009 and accepted February 1, 2010
† Kyushu Institute of Technology.
‡ Liaoning Institute of Technology.
§ Fukuoka University.
|| National Institute for Materials Science.
⊥ University of Tsukuba.
Kyushu Kyoritsu University.
DOI: 10.1021/am9006676

for as-deposited ITO films grown by dc-plasma sputtering without any intentional substrate heating (15). Both preservation of periodical electronic band structure of In_2O_3 crystal lattice and proper concentration of oxygen vacancy accommodated in the lattice are indispensable for realization of the highest conductivity with high transparency for the as-deposited films of hydrogen-doped ITO without any intentional substrate heating.

X-ray photoelectron spectroscopy (XPS) is suitable to examine in detail the valence states of ITO films sputter deposited in working gas containing hydrogen without any heat treatments. Since hydrogen radical generated in plasma is a strong reducing species (16), the radical reached the substrate surface in the deposition brings about not only oxygen vacancy and an oxygen−indium vacancy pair but also a hydroxyl−indium bond due to hydrogen resided in the film. Limpijumnong et al. (14) reported that the 1+ charged hydrogen at the interstitial sites prefers to be near the anions, and then, the O−H bond lengths in In_2O_3 are slightly longer than that in H_2O. The oxygen of such a hydroxyl−indium bond is represented as O^-, which gives rise to the suboxide-like oxygen O 1s peak in XPS. Usually, the suboxide-like O 1s peak appears at the higher-binding energy side than the lattice oxygen (O^{2-}). No O 1s peak from both oxygen vacancy and oxygen−indium vacancy pair is seen in XPS; therefore, we anticipate observing a doublet peak for the O 1s electrons. Further, we expect occurring of simultaneous growth and reduction of the O 1s peaks located respectively at the higher- and the lower-binding energy sides with increasing the hydrogen concentration in the gas. Of course, the O^- state lowers efficiency of the carrier doping using the O^{2-} vacancy in the lattice and increases density of the ionized scattering center for the carriers. An increase in the O 1s peak intensity ratio of the suboxide-like oxygen to the lattice oxygen implies lowering in both the carrier density and the mobility for the as-deposited films of hydrogen-doped ITO grown without substrate heating.

Rutherford backscattering spectroscopy−elastic recoil detection analysis (RBS−ERDA) is the most suitable for quantitative analysis of hydrogen resided in the film. As mentioned above, we assumed that the hydroxyl−indium bond in the film is originated from the resided hydrogen, and the O 1s peak intensity of the suboxide-like oxygen grows in proportion as the concentration of the resided hydrogen rises. Such an assumption can be proved by observation of parallelism between change in the suboxide-like O 1s peak intensity and that in the concentration of hydrogen resided in the as-deposited film. We employed RBS−ERDA for quantification of hydrogen in the as-deposited film and observed the parallelism between the suboxide-like O 1s peak intensity and the concentration of hydrogen resided in the films.

The suboxide-like O 1s peak accompanied by the lattice oxygen peak mirrors the electronic states of hydroxyl−indium bond added to the valence band of In_2O_3 crystal. The electronic band structure of In_2O_3 crystal can be considered only theoretically because we never obtain an experimentally perfect crystal and a perfect surface of In_2O_3. Therefore, we also employed the first-principles band structure calculation using the WIEN2k package (17) for consideration of changes in the valence band spectra of the as-deposited films with the hydrogen concentration in the gas. The calculation revealed that bonding hybridization between the oxygen p and the indium s orbitals formed the bottom of the valence band at 6−4 eV. The oxygen p component dominated the density of states ranging from 4 to 0 eV, at which the indium p state also contributed sparsely. The valence band structure of the as-deposited film grown with hydrogen of 1% was typical to that of the In_2O_3 crystal. The additional electronic structure above 4 eV, observed prominently in the valence band of the as-deposited films with hydrogen more than 1% in the gas, was attributed to the O^- state of oxygen in the hydroxyl−indium bond.

EXPERIMENT AND BAND STRUCTURE CALCULATION

dc-Plasma Deposition. Films of ITO were deposited on a glass substrate by dc-plasma sputtering of a sintered target (Kojundo Chemical, Japan) in working gas containing hydrogen. The target consisted of In_2O_3 (95 wt %) and SnO_2 (5 wt %). For the deposition, deuterium gas (99.99% purity) was introduced to the deposition chamber of the base pressure $\approx 1 \times 10^{-7}$ Torr with argon gas (99.9999% purity). It is well-known that protium related species such as $^1H_2$ and ^1H_2O molecules are usually involved in residual gas of vacuum systems, although we denoted the gas pressure ratio of deuterium to argon as the hydrogen concentration [D] in the gas. The [D] value was in the range of 0−3.6% for the deposition. The film thickness was ≈200 nm. Transmission electron microscopy for cross-sectioned specimens revealed that the films deposited with [D] ≤ 1.5% had monolithic structure and that with [D] = 3.6% had the structure of agglomerated spherical grains. X-ray diffraction demonstrated that the films had randomly oriented polycrystalline structure. Heat treatments such as substrate heating and postdeposition heating in air were eliminated to scrutinize changes in the valence states of oxygen of the films in relation to the [D] value in the deposition.

XPS and RBS−ERDA. The core and valence electrons were excited with monochromatized Al Kα radiation (1486.6 eV). The In $3d_{5/2}$, Sn $3d_{5/2}$, O 1s, and valence band spectra were recorded with a hemispherical electron spectrometer (ULVAC-PHI model-1800 L) in vacuum pressure less than 4.9×10^{-9} Torr at room temperature. The probing area at the sample surface and the electron takeoff angle were set to 800 μm^{Φ} and 45°, respectively. The spectrometer was calibrated using the Au $4f_{7/2}$ (84.0 eV) electrons. The full width at half-maximum of the Au $4f_{7/2}$ peak, as an indicator of resolution of the spectrometer, was 0.83 eV. The estimated electron energy uncertainty was ±0.15 eV in this experiment. Since all the samples were highly conductive, suddenly appeared core-hole can be readily screened by flows of densely populated n-type carriers.

Hydrogen (H and D) atoms resided in the samples were quantified by the RBS−ERDA method using the Tandem Accelerator installed at UTTAC in University of Tsukuba, Japan. Ions of He^+ accelerated up to 2.5 MeV were injected at the angle of 15° to the sample surface. The recoiled ions (H and D) and the backscattered ions (He) were collected by the detectors set at the angles of 30° and 150° with respect to the beam direction, respectively.

Band Structure Calculation. In_2O_3 crystallizes to form the C-type rare-earth structure with cubic cell lattice constant of 1.0118 nm (18). The space group symmetry of the unit cell is

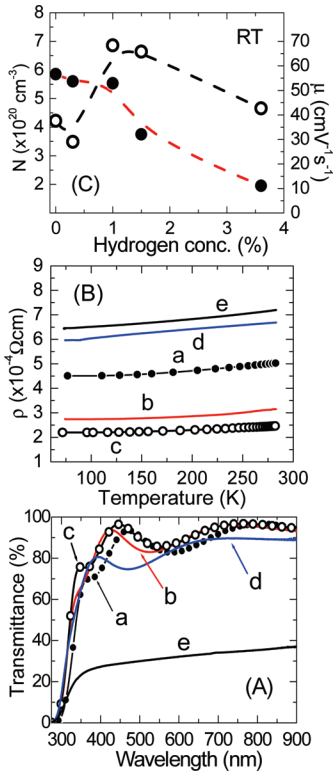

FIGURE 1. Optical transmittance spectra measured with a JASCO V-550 ultraviolet−visible spectrometer (A), and temperature dependence of resistivity ρ measured with a two probe method (B) of the samples deposited with [D] of 0 (a), 0.3 (b), 1 (c), 1.5 (d), and 3.6% (e). Carrier density N (open circle in the left-hand scale) and mobility μ (closed circle in the right-hand scale) of the samples measured with van der Pauw method at room temperature as a function of the [D] value (C).

$Ia\bar{3}$, and it contains 16 In_2O_3 formula units with fluorite-type unit cells accompanying systematic oxygen vacancies: indium atoms occupy Wyckoff positions 8b and 24d, and oxygen atoms occupy Wyckoff position 48e. In the unit cell, both 8a and 16c Wyckoff positions are empty, so 24 unoccupied sites are contained with 16 formula units of In_2O_3. The first-principles calculation was carried out to examine the electronic structure of In_2O_3. The calculation was performed using the WIEN2k code, which is based on the APW + lo method (17). We used the generalized-gradient approximation for the density functional theory. Muffin-tin radii R were chosen as 1.93 au for indium and oxygen, and the cutoff wavenumber K for basis functions was set to be $RK = 7.0$. The number of k-points in an irreducible Brillion zone was chosen as 400. With these parameters, sufficient numerical convergences were achieved.

RESULTS AND DISCUSSION

Optical and Electrical Properties. The samples deposited with [D] < 1.5% are transparent to the eye but that with [D] = 3.6% looks grayish. Optical transmittance in the visible wavelength region was ≥80% for the samples with [D] < 1.5% but that with [D] = 3.6% was ≈35%, as shown in Figure 1A. Energy dispersive X-ray spectroscopy with scanning transmission electron microscopy demonstrated that the distribution of indium and that of oxygen for the cross-sectioned sample of [D] = 3.6% are inconsistent with each other and suggested that hydrogen in the working gas led to reduction of ITO. Secondary electron microscopy revealed that the hydrogen definitely affected the surface morphology of the samples. The film surface became smoother with increasing [D] to 1%, but nucleation and growth of grains were apparent above [D] = 1.5%. Randomly oriented and agglomerated spherical grains were observed for the sample with [D] = 3.6%, which can give rise to enlargement of diffuse scattering at the film surface and then reduce the optical transmission of the film. Such a decrease in the transmittance with the sample with [D] = 3.6% can result from an enlargement of reflection at the film surface and can be due to the metallic indium component distributed randomly in the film.

As shown in Figure 1B, the sample with [D] = 1% demonstrated the lowest resistivity at room temperature and almost flat temperature-dependence of resistivity. Koida et al. (12) reported that both the carrier density and the mobility of the as-deposited In_2O_3 films were temperature independent. Such a high conductivity and a high transparency would be the result from both well preserved In_2O_3 band structure and proper concentration of the O^{2-} vacancy in the lattice. The carrier density versus [D] plot exhibited an inverse V-shaped behavior peaked at [D] = 1%, as shown by the Figure 1C. The mobility stayed almost constant below [D] = 1% but dropped rather rapidly above [D] = 1%. The sample with [D] = 1% exhibited the carrier density of ≈7 × 10^{20} cm^{-3} and the mobility of ≈50 $cm^2(Vs)^{-1}$. As it was expected, the carrier density of the ITO film was larger than that reported for the In_2O_3 film (12), while the mobility of the ITO film is almost the same as the reported one (12).

It is well-known that lattice defects resulting in mobile carriers of ITO are generally ionized, and they scatter carriers strongly (19−23). Both a low carrier density and a high mobility for the samples with [D] = 0 and 0.3% suggest that the hydrogen with a low concentration resulted predominantly in oxygen−indium vacancy pairs which form neutral defects in the crystal (24). The low density neutral defects scarcely affected carrier transport of the samples with [D] below 1%. Judging from both rather high carrier density and low mobility for the samples with [D] = 1.5 and 3.6%, the hydrogen generated not only the doubly charged oxygen vacancies (25) sufficient for prevailing over the neutral defect formation but also singly charged impurities due to hydrogen at the interstitial sites and/or hydrogen substituted for the oxygen sites in In_2O_3 (12−14).

An increase in the carrier density with [D] was expected from a simple assumption of the lattice oxygen withdrawal by hydrogen radical, while the carrier density decreased with [D] above 1%. Therefore, hydrogen resided in the samples, and then the hydrogen formed an hydroxyl−indium bond giving rise to the O^- state. The O^- state lowers the efficiency of carrier doping and increases the density of the ionized scattering center.

XPS. The observed spectral features in XPS are usually labeled in terms of one-electron quantum numbers despite photoemission from a solid is evidently a many-body process. The photoelectron binding energy E_B of a level j, $E_B(j)$, is the difference in the total energy of the system in its ground state and in the state with one electron missing in

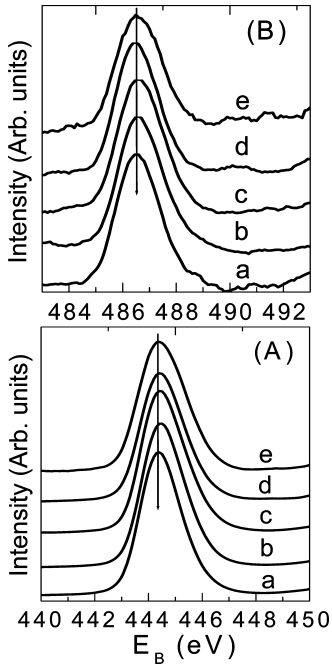

FIGURE 2. In $3d_{5/2}$ (A) and Sn $3d_{5/2}$ (B) spectra of the samples deposited with [D] of 0 (a), 0.3 (b), 1 (c), 1.5 (d), and 3.6% (e). The arrows are guides for the eye.

the orbital j and can be expressed as $E_B(j) = -\varepsilon(j)$ from Koopmans' theorem, where ε is the orbital energy. Therefore, shifts of $E_B(j)$ with changes in the chemical and/or physical states can be written as $\Delta E_B(j) = -\Delta\varepsilon(j)$. For most situations encountered in XPS, the equation is so close enough to discuss the shifts reflecting changes in the electronic states of the samples.

As shown in Figure 2A,B, E_Bs of the In $3d_{5/2}$ and Sn $3d_{5/2}$ levels stayed at 444.4 and 486.6 eV, respectively, notwithstanding the change in [D] from 0 to 3.6%. Within the experimental uncertainty, the In $3d_{5/2}$ E_B agreed well with those reported (26−30), and the Sn $3d_{5/2}$ E_B agreed well with those reported (16, 30). Such invariance in the In $3d_{5/2}$ and Sn $3d_{5/2}$ E_Bs regardless of the variation in [D] suggests that the periodic electronic band structure of In_2O_3 crystal lattice was scarcely affected by hydrogen in working gas for dc-plasma sputter deposition of ITO films without intentional substrate heating.

As shown in Figure 3, the samples exhibited two kinds of the peaks in the O 1s spectra. They demonstrated a systematic change in intensity with [D]. The lower E_B side peak at 530.0 eV, originated from the lattice oxygen (27−30), became less intense with increasing [D]. The higher E_B side peak, positioned at 531.8 eV for the samples a−c, at 531.5 eV for the sample d, and at 532.0 eV for the sample e, is the result from the suboxide-like oxygen (29, 30), and its intensity increased with increasing [D]. Figure 4 shows that the atomic ratio of lattice oxygen to indium was ≈1.5 for the sample with [D] = 0%, while for the samples with [D] = 0.3−3.6% the value decreased to ≈1.1 and stayed almost constant despite the variation of [D]. The intensity ratio of the suboxide-like oxygen to the lattice one increased almost linearly with [D] below 1.5% but grew rather rapidly at [D] = 3.6%. The growth of the suboxide-like oxygen at [D] =

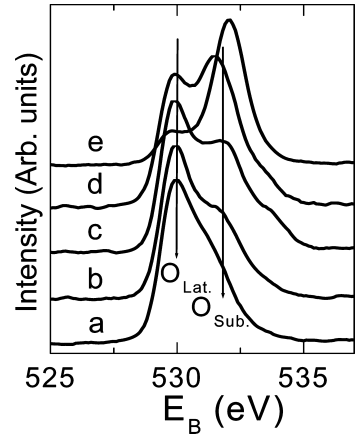

FIGURE 3. O 1s spectra of the samples deposited with [D] of 0 (a), 0.3 (b), 1 (c), 1.5 (d), and 3.6% (e). The arrows are guides for the eye.

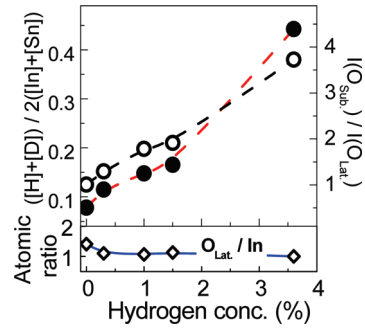

FIGURE 4. Atomic ratio of the lattice oxygen to indium (lower panel) and the O 1s peak intensity ratio of the suboxide-like oxygen to the lattice oxygen by XPS (closed circle in the right-hand scale) and the atomic ratio of hydrogen [H] + [D] to metal [In] + [Sn] by RBS−ERDA (open circle in the left-hand scale) of the samples as a function of the [D] value (upper panel).

3.6% reflects an increase of adsorbed hydrogen due to enlarged effective surface area by the structure consisted of agglomerated spherical grains. The growth in intensity of the suboxide-like oxygen suggests that resided hydrogen forms a hydroxyl−indium bond, and the intensity of suboxide-like oxygen corresponds to the population of the resided hydrogen.

RBS−ERDA. Therefore, we examined the concentration of hydrogen resided in the samples by the use of RBS−ERDA. Although the concentrations of protium and deuterium in the sample were quantified separately by RBS−ERDA, we employed the sum of the population of protium and deuterium as a parameter of the concentration of hydrogen in the sample. Both protium and deuterium form a similar hydroxyl−indium bond, and the concentration of deuterium is much higher than that of protium. Figure 4 also indicates that the concentration of the resided hydrogen in the sample correlated almost linearly to the [D] value. The change in the concentration of resided hydrogen was almost parallel to that in the intensity of suboxide-like oxygen. Thus, the suboxide-like O 1s peak originated from the resided hydrogen indicates an addition of the electronic structure of oxygen in the hydroxyl−indium bond to that of ITO. The electronic structure of the O^- state, which is overlapping with the valence band of the In_2O_3 crystal, grows with increasing [D].

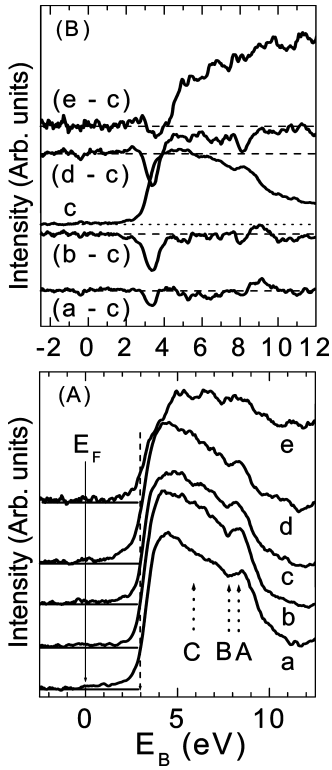

FIGURE 5. Valence band spectra (A) of the samples deposited with [D] of 0% (a), 0.3% (b), 1% (c), 1.5% (d), and 3.6% (e), and their difference spectra (B) relative to the sample c. For obtaining the difference spectra, the intensity of the valence band was normalized by the In 4d peak (18.2 eV) before subtraction. The arrows and horizontal lines are guides for the eye.

Electronic Structure. As shown by the Figure 5A, the samples demonstrated changes in the valence band spectra with [D], which were anticipated as a consequence of changes in the O 1s spectra. Both the onset and the hump positioned at 3 eV and at the Fermi energy E_F, respectively, of the valence band spectra are consistent with n-type conductivity for all the samples. The samples a−d deposited with [D] < 1.5% showed the peak noted as A in the figure at around 8.3 eV. The energy of the peak A varied with [D]; 8.6 eV for [D] = 0%, 8.4 eV for [D] = 0.3%, 8.1 eV for [D] = 1%, and 8.3 eV for [D] = 1.5%. The samples a−d showed also the valley noted as B in the figure at 7.7 eV. The energy of the valley B was independent of the [D] value. Only the sample c deposited with [D] = 1% exhibited the dip denoted as C in the figure at 5.8 eV. The sample e deposited with [D] = 3.6% showed a rather complicated structure which can be partitioned into two components; the component similar to the sample c and that above 4 eV which gradually increases in intensity with E_B, as shown by the difference spectrum (e−c) in Figure 5B. The valence band structure of the In_2O_3 crystal mentioned below was apparently smeared by the additional structure above E_B = 4 eV originated from the O^- state. Even in the sample d deposited with [D] = 1.5%, we see the structure above 4 eV, as shown by the difference spectrum (d−c) in Figure 5B. The difference spectra b−c and a−c in Figure 5B showed no structure above 4 eV additional to the valence band spectrum of the sample c. The samples deposited with [D] above 1% demonstrated changes in the electronic structure reflecting the concentration of hydrogen resided in the samples. The change in the valence band is consistent to but is less sensitive than that in the O 1s peak. Such a discrepancy in sensitivity for the change is based on the photoionization cross section of the wave functions. The cross section of the O 1s, O 2p, and In 5s levels are 0.40×10^5, 0.24×10^3, and 0.10×10^4 burn, respectively, in excitation with Al Kα radiation (31).

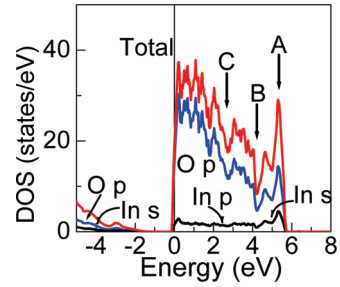

FIGURE 6. Calculated DOS of In_2O_3 crystal. The top of the valence band was set to zero in the energy scale. The energy scale is inverted so that DOS can be directly compared with XPS spectra in Figure 5.

Figure 6 shows the calculated density of states (DOS) of the In_2O_3 crystal. While the local-density approximation failed to reproduce the band gaps of semiconductors and insulators, the approximation succeeded to describe the valence and conduction bands of various compounds. In In_2O_3 crystal bonding hybridization between the oxygen p and the indium s orbitals formed the bottom of the valence band (below 4 eV). The oxygen p component dominated the DOS ranging from 4 to 0 eV, at which the indium p state also contributed sparsely. The conduction band above −1 eV consisted of the oxygen p and the indium s orbitals with antibonding hybridization.

Similar to the experimental valence band spectra shown in Figure 5A, we see the features A, B, and C even in the calculated DOS in Figure 6. The peak A in the total DOS, consisted of the oxygen p and the indium s bonding states, was positioned at 5.3 eV. The valley B in the total DOS, reflected predominantly the valley in the oxygen p partial DOS, was located at 4.2 eV. The dip C in the total DOS was due to the dip in the oxygen p partial DOS and was positioned at 2.7 eV. When we move the onset of the DOS by +3 eV for comparison with the experimental spectra of the samples with n-type conduction, the features A, B, and C are located at 8.3, 7.2, and 5.7 eV, respectively. Each of the features in the theoretical DOS agrees with that in the experimental spectrum of the sample c (A: 8.1 eV, B: 7.7 eV, and C: 5.8 eV) in Figure 4A. Therefore, the oxygen p and the indium s and p states hybridized well in the sample c. The periodic electronic band structure of the In_2O_3 crystal was well preserved in the sample deposited with [D] = 1%.

CONCLUSIONS

In XPS of ITO films dc-plasma sputter-deposited in working gas containing hydrogen, the core-level electrons of indium and tin showed no change in spite of variation of

[D], while the O 1s and the valence band electrons exhibited systematic spectral changes with [D]. The suboxide-like oxygen and the lattice oxygen corresponded to the components at the higher and lower E_B sides of the doublet O 1s peak. The suboxide-like oxygen peak grew and the lattice oxygen peak diminished simultaneously as the [D] value increased.

RBS−ERDA revealed that hydrogen resided in the samples increased with increasing [D] in the deposition, and the growth of the suboxide-like O 1s peak is parallel to the increase of the resided hydrogen. Therefore, hydrogen in the working gas resided in solids at almost a constant rate and then formed a hydroxyl−indium bond represented as the O^- state.

The spectral intensity above 4 eV in the valence band increased with the [D] value. The electronic structure is additional to that of In_2O_3 crystal and corresponds to the O^- state. The first-principles band structure calculation revealed that the sample deposited with [D] = 1 % preserved well the periodic band structure of In_2O_3. Although the samples deposited with [D] < 1 % indicated no electronic structure of the O^- state, the samples deposited with [D] > 1 % exhibited the additional structure due to the O^- state overlapping with the valence band of the sample deposited with [D] = 1 %.

Growth of the suboxide-like O 1s peak is consistent with that of the electronic structure of the O^- state. The O^- state originated from the resided hydrogen lowered the efficiency of carrier doping using the O^{2-} vacancy in the lattice and increased the density of ionized scattering center for the carriers. Both well preserved In_2O_3 band structure and proper concentration of the O^{2-} vacancy are indispensable for achieving a high conductivity and a high transparency of ITO.

Acknowledgment. The authors thank Dr. H. Shimooka of Kyushu Institute of Technology for assistance and Dr. H. Naramoto and the staff members of UTTAC at the University of Tsukuba for the RBS−ERDA experiment.

REFERENCES AND NOTES

(1) Salehi, A. *Thin Solid Films* **1998**, *324*, 214.
(2) Sheu, J. K.; Su, Y. K.; Chi, G. C.; Jou, M. J.; Chang, C. M. *Appl. Phys. Lett.* **1998**, *72*, 3317.
(3) Lewis, B.; Paine, D. *MRS Bull.* **2000**, *25*, 22.
(4) Ginley, D.; Bright, C. *MRS Bull.* **2000**, *25*, 15.
(5) Granqvist, C. G.; Hultaker, A. *Thin Solid Films* **2002**, *411*, 1.
(6) Lany, S.; Zunger, A. *Phys. Rev. Lett.* **2007**, *98*, 045501.
(7) Shigesato, Y.; Koshi-ishi, R.; Kawashima, T.; Ohsako, J. *Vacuum* **2000**, *59*, 614.
(8) Jun, S.-I.; McKnight, T. E.; Simpson, M. L.; Rack, P. D. *Thin Solid Films* **2005**, *476*, 59.
(9) Dewit, J. H. W. *J. Solid State Chem.* **1973**, *8*, 142.
(10) Dewit, J. H. W.; Vanunen, G.; Lahey, M. *J. Phys. Chem. Solids* **1977**, *38*, 819.
(11) Morikawa, H.; Fujita, M. *Thin Solid Films* **2000**, *359*, 61.
(12) Koida, T.; Fujiwara, H.; Kondo, M. *Jpn. J. Appl. Phys* **2007**, *46*, L685.
(13) King, P. D. C.; Lichti, R. L.; Celebi, Y. G.; Gil, J. M.; Vilão, R. C.; Alberto, H. V.; Duarte, J. P.; Payne, D. J.; Egdell, R. G.; McKenzie, I.; McConville, C. F.; Cox, S. F. J.; Veal, T. D. *Phys. Rev. B* **2009**, *80*, 081201(R) .
(14) Limpijumnong, S.; Reunchan, P.; Janotti, A.; Van De Walle, C. G. *Phys. Rev. B* **2009**, *80*, 193202.
(15) Luo, S.; Okada, K.; Kohiki, S.; Tsutsui, F.; Shimooka, H.; Shoji, F. *Mater. Lett.* **2009**, *63*, 641.
(16) Wallinga, J.; Bik, W. M. A.; Vredenberg, A. M.; Schropp, R. E. I.; van der Weg, W. F. *J. Phys. Chem. B* **1998**, *102*, 6219.
(17) Blaha, P.; Schwartz, K.; Madsen, G. K. H.; Kvasnicka, D.; Luitz, J. *WIEN2k, An Augmented Plane Wave + Local Orbitals Program for Calculating Crystal Properties*; Tech. Universitat Wien: Vienna, Austria, 2001.
(18) Marezio, M. *Acta Crystallogr.* **1966**, *20*, 723.
(19) Zhang, D. H.; Ma, H. L. *Appl. Phys. A: Mater. Sci. Process.* **1996**, *62*, 487.
(20) Chen, M.; Pei, Z. L.; Wang, X.; Yu, Y. H.; Liu, X. H.; Sun, C.; Wen, L. S. *J. Phys. D: Appl. Phys.* **2000**, *33*, 2538.
(21) Chen, M.; Pei, Z.; Wang, X.; Sun, C.; Wen, L. *Mater. Res. Soc. Symp. Proc.* **2001**, *666*, F2.3/1.
(22) Minami, T.; Suzuki, S.; Miyata, T. *Mater. Res. Soc. Symp. Proc.* **2001**, *666*, F1.3/1.
(23) Gilmore, A. S.; Al-Kaoud, A.; Kaydanov, V.; Ohno, T. R. *Mater. Res. Soc. Symp. Proc.* **2001**, *666*, F3.10/11.
(24) Ishibashi, S.; Higuchi, Y.; Ota, Y.; Nakamura, K. *J. Vac. Sci. Technol., A* **1990**, *8*, 1399.
(25) Banerjee, R.; Ray, S.; Basu, N.; Batabyal, A. K.; Barua, A. K. *J. Appl. Phys.* **1987**, *62*, 912.
(26) Wu, X. C.; Hong, J. M.; Han, Z. J.; Tao, Y. R. *Chem. Phys. Lett.* **2003**, *373*, 28.
(27) Sasaki, M.; Kiyoshima, R.; Kohiki, S.; Matsushima, S.; Oku, M.; Shisido, T. *J. Alloys Compd.* **2001**, *322*, 220.
(28) Sasaki, M.; Yasui, K.; Kohiki, S.; Deguchi, H.; Matsushima, S.; Oku, M.; Shisido, T. *J. Alloys Compd.* **2002**, *334*, 205.
(29) Lee, M.-S.; Choi, W. C.; Kim, E. K.; Kim, C. K.; Min, S.-K. *Thin Solid Films* **1996**, *279*, 1.
(30) Fan, J. C. C.; Goodenough, J. B. *J. Appl. Phys.* **1977**, *48*, 3524.
(31) Yeh, J. J.; Lindau, I. *At. Data Nucl. Data Tables* **1985**, *32*, 1.

AM9006676